Reaction Chemistry & Engineering

ROYAL SOCIETY OF CHEMISTRY

PAPER

View Article Online
View Journal | View Issue

Check for updates

Cite this: *React. Chem. Eng.*, 2020, 5, 2148

# Continuous hydrothermal leaching of $LiCoO_2$ cathode materials by using citric acid†

Qingxin Zheng, *[a] Kensuke Shibazaki,[b] Tetsufumi Ogawa,[b] Atsushi Kishita,[a] Yuya Hiraga,[a] Yuta Nakayasu [c] and Masaru Watanabe*[ad]

Received 9th July 2020,
Accepted 3rd August 2020

DOI: 10.1039/d0re00286k

rsc.li/reaction-engineering

The first run of continuous hydrothermal leaching of lithium-ion battery cathode materials, $LiCoO_2$, was performed using citric acid as the leachant at 200 °C. The flow system was specially designed and customized. Prior to the hydrothermal leaching experiments, a three-layer model was used to predict the flow state in this flow system, and a cold flow test using two kinds of flow lines was performed to determine the conditions in the preliminary experiments. Finally, the pulp density of the slurry and the flow rate were set to 10 g $L^{-1}$ and 30 ml $min^{-1}$, respectively, for the continuous hydrothermal leaching experiments. At 60 min after the start of slurry feeding, the leaching efficiency of Li and Co reached 81.3% and 92.7%, respectively, and can continue to increase with the extension of time. The successful run indicated that the process of hydrothermal leaching is feasible and promising to be applied in practice. Meanwhile, a problem of acid corrosion caused by the use of citric acid during this process was revealed and is expected to be resolved using inner coating materials with high acid corrosion resistance or organic acids with low or no acid corrosion as the leachant.

Published on 03 August 2020. Downloaded on 9/3/2025 6:59:12 AM.

## 1 Introduction

Due to their high voltage, high stability, long life, and light weight, lithium-ion batteries (LIBs) are being widely applied from portable electronic devices to electric vehicles.[1] To meet the global demand for power sources, the manufacture of LIBs is increasing greatly,[2] followed by huge consumption of various cathode materials used in LIBs and massive generation of spent LIBs.[3–5]

LIB cathode materials are usually composed of lithium-containing oxides of transition metals, such as $LiCoO_2$, $LiNiO_2$, $LiMn_2O_4$, $LiFePO_4$, $LiMnPO_4$, $LiCoPO_4$, and their mixtures.[4] The metal components in LIBs need a stable supply to meet the increasing consumption; however, some of them are mainly produced from a limited number of countries or geographically remote areas and thus have unstable supplies caused by geopolitical issues.[6,7] For example, about 70% of Co is produced by Congo (59%), Australia (5%), and Russia (7%).[8] The mining supply of metals, such as Li and Co, is predicted to reach their limits and will be exceeded by the demand soon. On the other hand, spent LIBs are regarded as a kind of hazardous solid waste, which would bring a tremendous burden on the environment and resource conservation.[2] Therefore, efficient recovery of valuable metals (*e.g.*, Li, Co, Ni, and Mn) from spent LIBs under mild conditions will be essential to conserve natural resources, reduce environmental problems, keep resource stability and security, and bring economic benefits.[9] As the first type of commercialized cathode material, $LiCoO_2$ has been widely employed in most commercial LIBs, and recently, the quantity of discarded $LiCoO_2$ has increased regularly and continuously.[10] Compared with other LIB materials, spent $LiCoO_2$ is always regarded as a worthy target for recycling because it is rich in Li and Co.[11]

Hydrometallurgy is one of the conventional methods for recovering metal components from spent LIBs in the lab and industry, composed of acid leaching in the first step and separation in the second step.[12,13] In the leaching stage, spent LIB cathode materials, such as $LiCoO_2$, $LiNiO_2$, and $LiMn_2O_4$, are converted to an aqueous solution of mixed metal ions. A traditional and well-known process is leaching metal ions with a mineral or an inorganic acid (*e.g.*, sulfuric acid or nitrate acid) in non-pressurized hot water.[14] Meanwhile, chemical reductants (*e.g.*, $H_2O_2$, $NaHSO_3$, or

[a] *Research Center of Supercritical Fluid Technology, Department of Chemical Engineering, Graduate School of Engineering, Tohoku University, 6-6-11 Aoba, Aramaki, Aoba-ku, Sendai, 980-8579 Japan.*
*E-mail: qingxin.zheng.a2@tohoku.ac.jp, masaru.watanabe.e2@tohoku.ac.jp*
[b] *Faculty of Environmental Studies, Tohoku University, 6-6-11 Aoba, Aramaki, Aoba-ku, Sendai, 980-8579 Japan*
[c] *Frontier Research Institute for Interdisciplinary Sciences, Tohoku University, 6-6-11-406 Aoba, Aza, Aramaki, Aoba-ku, Sendai 980-8578, Japan*
[d] *Environment Conservation Center, Department of Chemical Engineering, Graduate School of Engineering, Tohoku University, 6-6-11 Aoba, Aramaki, Aoba-ku, Sendai, 980-8579 Japan*

† Electronic supplementary information (ESI) available: Information of the linear fitting lines for the plots used in the kinetic study. See DOI: 10.1039/d0re00286k



This journal is © The Royal Society of Chemistry 2020

Published on 03 August 2020. Downloaded on 9/3/2025 6:59:12 AM.

$Na_2S_2O_3$)[15] are added to improve the leaching efficiency and lower the required concentration of acids. Due to its drawbacks in terms of high-concentration inorganic acids, consumption of reductants, batch-style apparatus, long time, and strong acid corrosion, the traditional leaching process always brings severe environmental pollution and economic burden. Therefore, making this process a greener and more environmentally-friendly step-by-step one is attracting increasing attention.

As shown in Scheme 1, looking for alternatives to inorganic acids is the first stage in the green progress of the acid leaching process for $LiCoO_2$. Compared to inorganic acids, organic acids are milder with lower acid corrosion and pollution. To date, there have been plenty of reports on the leaching of metal ions from spent LIB cathode materials using organic acids as the leachant, such as succinic acid,[16] malic acid,[17] aspartic acid,[17] citric acid ($H_3Cit$),[18–20] acetic acid,[21] lactic acid,[22] tartaric acid,[23] oxalic acid,[24] glycine,[25] and so on. These achievements have proved that organic acids could displace inorganic acids for the acid leaching process. However, reductants are still indispensable for reducing the transition metal ions from a high to a low state.[18] For example, without reductants, the leaching efficiencies of Li and Co decreased significantly, despite the use of inorganic or organic acids.[6,7,17,26]

To date, two feasible paths have been reported to avoid the consumption of additional reductants. The one is leaching with ascorbic acid.[27] During this process, ascorbic acid plays the roles of both a leachant and reductant. Another one was proposed in 2017, using pressurized hot water to leach Li and Co from $LiCoO_2$ with $H_3Cit$, and the process was also called 'hydrothermal leaching'.[26] Without using any reductant like $H_2O_2$, hydrothermal leaching with $H_3Cit$ (0.4 mol $L^{-1}$) achieved a leaching efficiency of 94% for both Li and Co at 200 °C for 10 min.[26] This good performance was attributed to $H_3Cit$ which supplies a proton, forms a soluble complex with Co, and shows reducibility even though $H_3Cit$ does not work as a reductant below 100 °C. Different from the traditional leaching process using non-pressurized hot water, the temperature of the hydrothermal leaching process is not limited by the boiling point of water at 100 °C. The use of high temperature greatly accelerates the reaction, shortens the reaction time, and decreases the required concentration of acid.[28] With a lower concentration of acids, no consumption of reductants, and a higher reaction rate, hydrothermal leaching is more efficient and environmentally friendly than the traditional leaching method, although an organic acid is used in each of them.

One of the next targets in the green progress is developing the leaching apparatus from a batch to a continuous flow system, which can enhance the productivity, reduce the processing time, improve the quality, have lower reagent and power consumption, save the costs, facilitate the scale-up, and move forward to the industrial application.[29,30] To our knowledge, continuous acid leaching of metal components from LIB cathode materials using a flow system has never been achieved in any conventional hydrometallurgy process, due to possible reasons such as the long reaction time and severe acid corrosion caused by the use of inorganic acids or high-concentration organic acids. Performed in pressurized hot water with low-concentration organic acids, the hydrothermal leaching method becomes one of the promising candidates to realize continuous leaching, but its development is still in the initial stage and the device is currently limited to the batch-style apparatus with a small scale. Therefore, at the current stage, a flow system, in which the hydrothermal leaching can be performed continuously, is urgently demanded.

In this study, we applied a specifically designed and customized flow system to perform the continuous hydrothermal leaching of $LiCoO_2$ using $H_3Cit$ as the leachant for the first time. The preliminary conditions such as the pulp density of the slurry and flow rate were determined based on the results of a three-layer model and a cold flow test without heating. During the first run of continuous hydrothermal leaching experiments, the experimental conditions were given in detail, the flow system was modified, the results of leaching efficiency were obtained, and problems such as acid corrosion as well as feasible resolutions were considered.

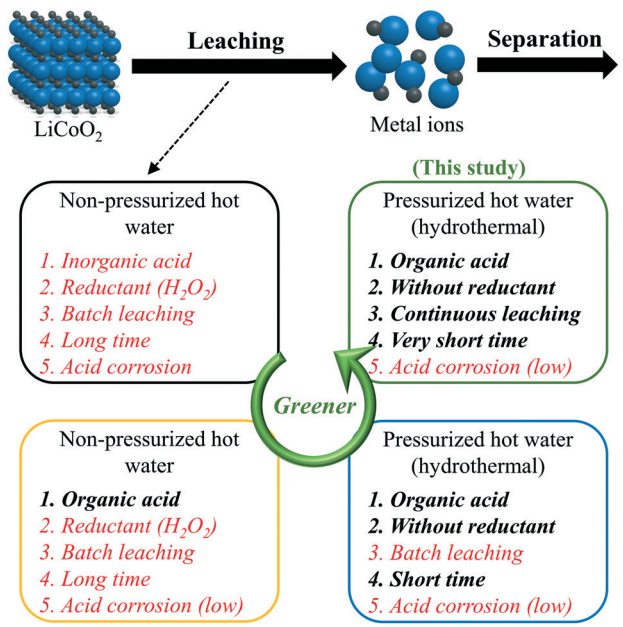


**Scheme 1** The green progress of the acid leaching process for $LiCoO_2$. The words marked in red color are the problems to be resolved.

## 2 Experimental

### 2.1 Reactants

A commercial LIB cathode material, $LiCoO_2$ (>98%, STREM Chemicals, layered rocksalt), and $H_3Cit$ (>99.5%, FUJIFILM Wako Pure Chemical) were purchased and used without

Published on 03 August 2020. Downloaded on 9/3/2025 6:59:12 AM.

further purification or treatment. Based on the light scattering results (Fig. S1†), the diameter of $LiCoO_2$ particles mainly distributed in the range of 5–40 μm. Ultra-pure water was supplied using a distillation apparatus (WG-220, Yamato Co.) and had a conductivity of 5.5 μS $m^{-1}$.

### 2.2 Apparatus

Scheme 2 shows the schematic diagram of a laboratory-scale continuous hydrothermal leaching system. Two feeding tanks (tank A and B, with a stirrer inside), a slurry pump (JASCO Corporation, PU-2100S), two pre-heaters (pre-heaters 1 and 2, twined by a piping tube and wrapped by a heat insulator), a reactor or sedimentation separator (SUS304, 1 inch; twined by four coil heaters and wrapped by a heat insulator), a cooler (SIBATA), a back-pressure regulator (JASCO, BP-2080-M), and a product collector were connected in series. The lines between the feeding tanks and the slurry pump were made of Teflon, and the other piping tubes (GL Sciences, 1/8 inch) and connectors (Swagelok) were made of stainless steel SUS316. The heaters (Hakko Electric, DGT0010) in the reactor from top to bottom were denoted as heater 1, heater 2, heater 3, and heater 4, respectively. In the reactor, the liquid and solid products were separated from the top and bottom, respectively. To restrain the sedimentation of solid particles in the slurry, the position of the feeding tank is higher than the collector. Many thermocouples in the system were used to monitor the temperature conditions and control the heaters accurately.

### 2.3 Cold flow test

Prior to the hydrothermal leaching experiment, a flow test without heating (or cold flow test) was conducted to explore the initial conditions, such as the flow rate and pulp density. Here, two flow lines (A and B) were used for the flow test, as shown in Scheme 3. In a typical experiment, tanks A and B were filled with pure water and a mixed slurry of $LiCoO_2$/water (pulp density: 1–50 g $L^{-1}$), respectively. First, pure water was pumped into the system with a specific flow rate (10 or 30 ml $min^{-1}$). After confirming that the water reached the outlet, the supply of the pure water was stopped and the supply of the slurry began. After continuous flowing for 10 min, sampling was started and performed 6 times with an interval of 5 min. After evaporating the water, the solid product contained in the recovered solution could be obtained. The pulp density of the recovered solution was calculated using the weight of the slurry and the weight of the solid product contained in the slurry. Based on the pulp density of each recovered solution, the flowing or pumping stability was determined and evaluated.

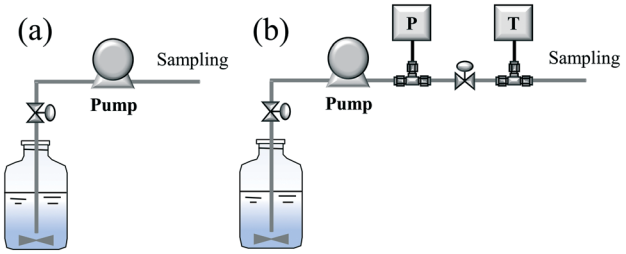


Scheme 3 Schematic diagrams of (a) flow line A and (b) flow line B for the cold flow test.

### 2.4 Continuous hydrothermal leaching of $LiCoO_2$ with $H_3Cit$

A 0.4 mol $L^{-1}$ $H_3Cit$ aqueous solution (>2 L) was prepared and placed in tank A. A slurry (pulp density: 10 g $L^{-1}$) was prepared by mixing 20 g of $LiCoO_2$ with 1980 g of 0.4 mol $L^{-1}$ $H_3Cit$ aqueous solution, and was placed into tank B. In a typical experiment, pure water was pumped to the system with a flow rate of 30 ml $min^{-1}$, and the system pressure was controlled to 20 MPa with the back-pressure regulator. In consideration of safety, the pressure was increased by 5 MPa at a time. After confirming that the system pressure was maintained and there was no liquid leakage from the system, heating was started. In this study, the leaching temperature was 200 °C, and the setting temperatures of pre-heaters and heaters were increased step by step, as shown in Table 1. The setting temperature of the heater at the bottom of the reactor was lower than that at the top. This is to restrain the density difference of the liquid due to the difference in temperature, which can generate convection in the reactor and reduce the separation performance, promote the precipitation of the unleached materials, and prevent the blocking at the outlet of the reactor.

After the temperature became unchanged, the supply of pure water was stopped, and the $H_3Cit$ aqueous solution was

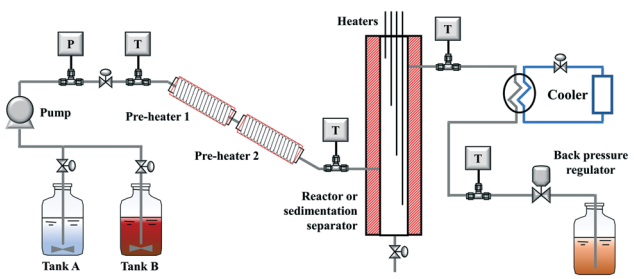


Scheme 2 The schematic diagram of the continuous hydrothermal leaching system.

Table 1 Setting temperature for each pre-heater or heater at different steps[a]

| | Step 1 | Step 2 | Step 3 | Step 4 | Step 5 | Step 6 |
|---|---|---|---|---|---|---|
| Pre-heater 1 | 150 | 180 | 180 | 200 | 200 | 200 |
| Pre-heater 2 | 150 | 180 | 180 | 200 | 200 | 200 |
| Heater 1 | 100 | 125 | 150 | 180 | 200 | 200 |
| Heater 2 | 100 | 125 | 150 | 180 | 200 | 200 |
| Heater 3 | 70 | 100 | 125 | 150 | 180 | 195 |
| Heater 4 | 40 | 80 | 100 | 120 | 150 | 190 |

[a] The preheaters or heaters were heated step by step to the specific temperatures.


This journal is © The Royal Society of Chemistry 2020

Published on 03 August 2020. Downloaded on 9/3/2025 6:59:12 AM.

supplied into the system from tank A. After about 15 min, the water in the system was completely displaced by the $H_3Cit$ solution. After confirming that the pressure was maintained, there was no leakage, and the heating was stable, the supply of the $H_3Cit$ aqueous solution was stopped, and the supply of the slurry was started. During the experiment, the slurry in the feeding tank was stirred at a speed of 600–800 rpm using a 4-blade stirrer (AS ONE, SM-101) to suppress solid–liquid separation. Sampling was started after the slurry was fed for 15 min, and performed 10 times with an interval of 5 min.

### 2.5 Analyses and definition

The size distribution of raw LIB material $LiCoO_2$ was obtained using a particle size analyzer (MT3300EXII, Microtrac). The composition of metal ions in the leachate was qualified and quantified by inductively coupled plasma atomic emission spectroscopy (ICP-AES; iCAP6500, Thermo Fisher), in which the wavelengths for identifying Li and Co were 670 and 228 nm, respectively. Before the ICP test, the solution was diluted to 1/200.

Leaching efficiency is defined as the percentage of the mass of the metal ion in the recovered solution against the total mass of the metal ion in the starting material. The calculation equation (eqn (1)) is shown as follows.

$$\text{Leaching efficiency} = \frac{\text{Metal ion in leachate}[g]}{\text{Metal ion in feedstock}[g]} \times 100\% \quad (1)$$

### 2.6 Three-layer model

In this study, a three-layer model was used to predict the characteristics of the solid–liquid flow (slurry flow). As supposed in the three-layer model and shown in Scheme 4,[31] when a solid–liquid mixture flows in a horizontal pipe at a given flow rate, three layers exist in the pipe: a stationary bed (SB layer) at the bottom, a moving bed (MB layer) above it, and a heterogeneous suspended flow (H layer) at the top. The detailed formula derivation process follows a previous report,[32] and is described in the ESI.† Finally, a flow pattern map, which expresses the relationship between the pulp density and the flow rate of the $LiCoO_2$ slurry, was constructed and used to predict the flow state of the slurry and set the conditions under which accumulation or deposition does not occur.

## 3 Results and discussion

### 3.1 Cold flow test

The results of cold flow tests without heating were obtained to determine the conditions in the further continuous leaching experiments, mainly the flow rate and pulp density.

**3.1.1 Flow line A.** Fig. 1 shows the effect of time on the pulp density of the recovered solution using flow line A at a flow rate of 10 ml $min^{-1}$. A higher initial pulp density is more possible to cause the accumulation of particles, and the variation of the pulp density of the recovered solution is usually regarded as one of the most important criteria to assess the occurrence of the accumulation. When an accumulation occurs, the pulp density of the recovered solution would go down first; along with the continuous injection of the slurry, the accumulated $LiCoO_2$ particles would be carried quickly after a critical point, like a dam burst, resulting in a rapid rise of the pulp density of the recovered solution. When the pulp density of the feeding slurry was 10 g $L^{-1}$, the recovered solution had a maximum pulp density of around 10 g $L^{-1}$. Even though the pulp density of the recovered solution dropped after 35 min, the results were enough to prove that a stable feeding was possible. On the other hand, when the pulp density of the feeding slurry was 50 g $L^{-1}$, the pulp density of the recovered solution was 30–80 g $L^{-1}$, showing a large variation.

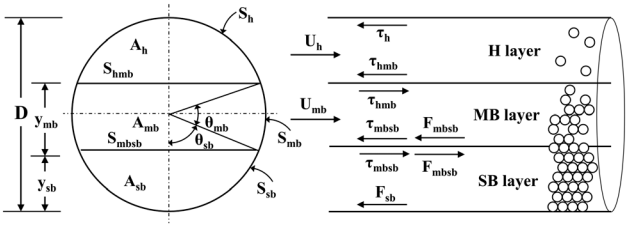


**Scheme 4** Schematic diagram of the three-layer model. Here, the H layer is a heterogeneous flow; the MB layer is a moving bed; the SB layer is a stationary bed; $D$ is the pipe diameter; $y_{mb}$ and $y_{sb}$ are the heights of the MB and SB layers, respectively; $A_h$, $A_{mb}$, and $A_{sb}$ are the cross-sectional areas occupied by the H, MB, and SB layers, respectively; $S_h$, $S_{mb}$, and $S_{sb}$ are the contact surfaces of the pipe wall with the H, MB, and SB layers, respectively; $S_{hmb}$ is the interface between the H and MB layers; $S_{mbsb}$ is the interface between the MB and SB layers; $\theta_{mb}$ and $\theta_{sb}$ are the central angles associated with $y_{mb}$ and $y_{sb}$; $U_h$ and $U_{mb}$ are the mean velocities of the H and MB layers, respectively; $\tau_h$ and $\tau_{hmb}$ are the upper layer shear stress and the interfacial shear stress acting on $S_h$ and $S_{hmb}$, respectively; $\tau_{mbsb}$ and $F_{mbsb}$ are the hydrodynamic shear stress and the dry friction force acting on $S_{mbsb}$, respectively; $F_{sb}$ is the dry friction force acting on $S_{sb}$.

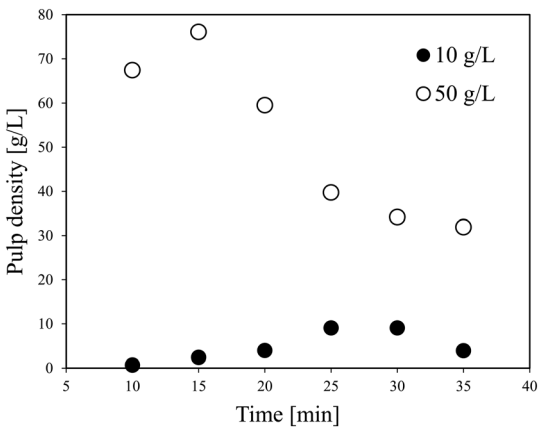


**Fig. 1** Effect of time on the pulp density of the recovered solution using flow line A.

Published on 03 August 2020. Downloaded on 9/3/2025 6:59:12 AM.

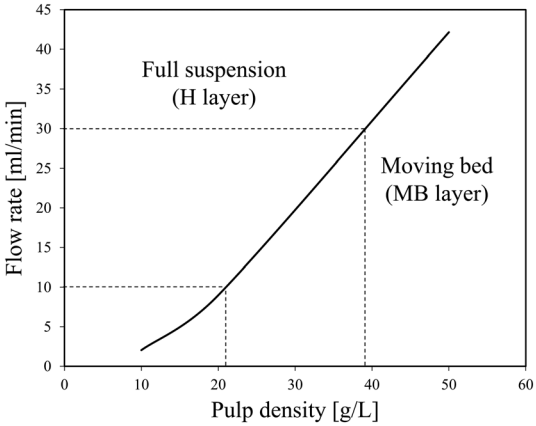


Fig. 2 Flow pattern map of the $LiCoO_2$ slurry.

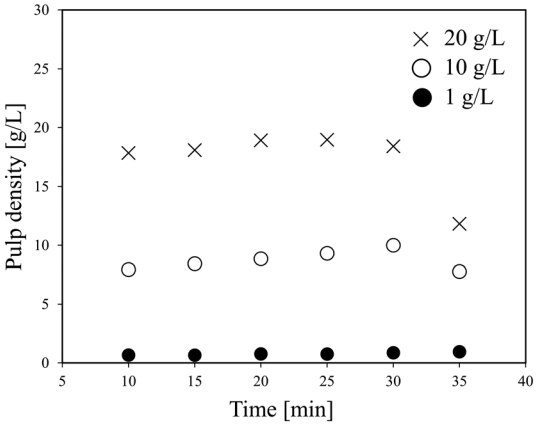


Fig. 3 Effect of time on the pulp density of the recovered solution using flow line B ($LiCoO_2$, 30 ml $min^{-1}$).

Particularly, the pulp density of the recovered solution at each time of 10, 20, and 30 min is higher than the initial pulp density of 50 g $L^{-1}$. In addition, after the completion of the experiment, the inside of the tube was washed and a large amount of $LiCoO_2$ particles were recovered. This evidence revealed agglomeration of the $LiCoO_2$ particles. It was speculated that the pumping became insufficient with increasing pulp density of the feeding slurry, simultaneously with the deposition of solid particles in the tube.

Fig. 2 shows the relationship between the pulp density and the flow rate of the $LiCoO_2$ slurry calculated using the three-layer model. The density of $LiCoO_2$ is 5000 kg $m^{-3}$, and the average particle size is 12.4 μm based on the particle size distribution shown in Fig. S1.† The density ($\rho_L$) and viscosity ($\mu_L$) of the $H_3Cit$ aqueous solution were assumed to be similar to those of water. The viscosity of the slurry ($\mu_s$) was assumed to be similar to that of water. In Fig. 2, the area above the solid line represents the full suspension area (H layer), where the liquid flows without forming a deposit, and the bottom area is the moving bed area (MB layer) that is transported while forming a deposit. From Fig. 2, it was found that at a flow rate of 10 ml $min^{-1}$, the slurry can be transferred without deposition when the pulp density was less than about 21 g $L^{-1}$, while at a pulp density of 50 g $L^{-1}$, the $LiCoO_2$ particles can deposit in the tube, making a stable liquid transfer difficult to achieve. This gave a good explanation for the experimental results shown in Fig. 1.

**3.1.2 Flow line B.** To get closer to the actual outline, a cold flow test using flow line B was described here. From the viewpoints of suppressing the deposition and improving the operability, the flow rate was increased from 10 to 30 ml $min^{-1}$. In addition, to further suppress the accumulation, the feeding tanks were moved at a higher position than the product collector, so that the flow from the feeding tank to the product collector was not against gravity, and the pipe was arranged to go down gradually.

Fig. 3 shows the effect of time on the pulp density of the recovered solution using flow line B. When the pulp density of the slurry was 1 g $L^{-1}$, the recovered solution has a stable pulp density in each of the six samplings. When the slurry pulp density increased to 10 or 20 g $L^{-1}$, the pulp density of the recovered solution was stable in the first five samplings, but then dropped in the 6th time. Particularly at a slurry pulp density of 20 g $L^{-1}$, the pulp density of the recovered solution in the 6th sampling decreased a lot to almost a half. From Fig. 2, under the conditions of 10 or 20 g $L^{-1}$ (pulp density of the feeding slurry) and 30 ml $min^{-1}$ (flow rate), it is in the full suspension range and accumulation should not occur. The conflict again illustrates the difference between the theoretical model results and the actual experimental results. A possible reason for the decrease in the 6th time is that the particles accumulate in the slurry pump as time elapses from the start of the slurry feeding, and then the feeding performance is impaired. The $LiCoO_2$ particles might deposit in the slurry pump and cause blockage, thereby lowering the transfer rate. That is, it can be expected that a long-term operation will be difficult for this flow system when the pulp density of the slurry is high.

Based on the above results, the pulp density of the slurry and the flow rate were set to 10 g $L^{-1}$ and 30 ml $min^{-1}$, respectively, in the next continuous hydrothermal acid leaching experiments.

### 3.2 Continuous hydrothermal leaching of $LiCoO_2$ with $H_3Cit$

As the most expensive LIB cathode material with a large market share, $LiCoO_2$ was chosen to be the research target of the first-time continuous hydrothermal leaching process. The conditions for the preliminary experiments were decided according to the results of the three-layer model and cold flow test.

Fig. 4 shows the leaching efficiency of Li and Co at different times during the continuous hydrothermal leaching of $LiCoO_2$ with $H_3Cit$ (0.4 mol $L^{-1}$). At 15 min after the start of slurry feeding, which was the first sampling, the leaching efficiencies of Li and Co were 64% and 74%, respectively. Then, the leaching efficiency of the metals increased gradually with the extension of time, which can be attributed to the replacement of the $H_3Cit$ aqueous solution in the

 This journal is © The Royal Society of Chemistry 2020

Published on 03 August 2020. Downloaded on 9/3/2025 6:59:12 AM.

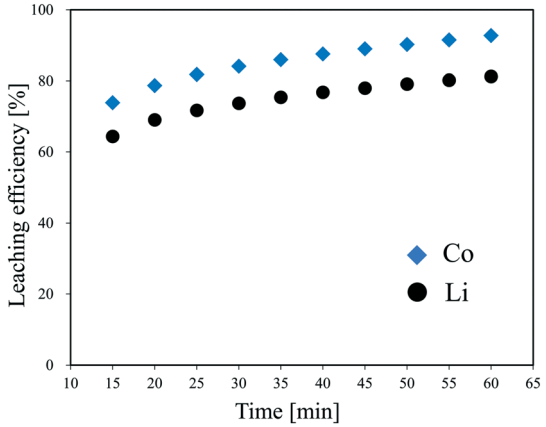


Fig. 4 Effect of time on the leaching efficiency of Li and Co during the continuous hydrothermal leaching of $LiCoO_2$ with $H_3Cit$.

system with the slurry being insufficient immediately after the switching. At 60 min, which was the 10th sampling, the leaching efficiency of Li and Co achieved 81.3% and 92.7%, respectively, approaching the data obtained using a batch-style apparatus at 15 min.[26] Therefore, the recovered solution or leachate with a high leaching efficiency can be collected continuously after 60 min of slurry feeding, even if the leaching efficiencies of Li and Co are expected to increase even after 60 min.

This is the first time to achieve continuous leaching of LIB cathode materials by a hydrothermal method. Even though the current conditions may be far from the optimum, the results are sufficient to prove the feasibility of the continuous hydrothermal leaching process and the applicability of this flow system.

### 3.3 Problem analysis during continuous hydrothermal leaching of $LiCoO_2$ with $H_3Cit$

As this is the first run of a flow system for hydrothermal leaching, problems existed inevitably. Problem analysis is beneficial to the improvement of this technology. One of the most obvious problems is that metal ions other than Li and Co were analyzed from the recovered solution.

Table 3 Elemental composition of the stainless steel used in the flow system[a]

| | Ni [wt%] | Mn [wt%] | Fe [wt%] | Cr [wt%] |
|---|---|---|---|---|
| SUS304 | 8–11 | <2 | 67–69 | 18–20 |
| SUS316 | 10–14 | <2 | 64–66 | 16–18 |

[a] The steel types include SUS304 and SUS316.

Table 2 shows the concentration of each metal ion in the recovered solutions at different times during hydrothermal leaching of $LiCoO_2$ with $H_3Cit$. Except for Li and Co, Ni, Fe, Cr, and a tiny amount of Mn were detected. As a pure $LiCoO_2$ compound was used in this study, the source of the other metal ions might be the steel materials used in the flow system. After comparing with the elemental composition of the stainless steel used in the flow system, SUS306 and SUS3016, as listed in Table 3, it can be inferred that the other metal ions must originate from the steel tubes used in the flow system. Additionally, the variation trend of the concentration with the extension of time was different for different metal ions. With the extension of time, the concentration of Li, Co, and Ni increased, while that of Mn, Fe, and Cr decreased first and then tended to be unchanged. This is probably because at the beginning of the reaction, $H_3Cit$ corrodes the pipe and then the wall of the tube is 'protected' by the accumulation of $LiCoO_2$ as the reaction proceeds.

The acid corrosion revealed here is an obvious problem in the further application, but its severity is much lower than that caused by the use of inorganic acids or high-concentration organic acids in the conventional leaching method. It is known that the acids must be used in all current leaching processes. Even though the corrosion caused by the acids cannot be eliminated completely, its damage is being reduced gradually in the green progress. For example, there are several feasible ways to avoid or suppress acid corrosion. One is to apply Teflon or coating materials with high acid corrosion resistance to the inner wall of the tubes. Another one is to choose organic acids with low or no acid corrosion as the leachant. In addition,

Table 2 The concentration of each metal ion in the recovered solutions at different times during the continuous hydrothermal leaching of $LiCoO_2$ with $H_3Cit$[a]

| Time [min] | Li [ppm] | Co [ppm] | Ni [ppm] | Mn [ppm] | Fe [ppm] | Cr [ppm] |
|---|---|---|---|---|---|---|
| 15 | 472.9 | 4553.2 | 103.7 | 7.9 | 301.0 | 85.5 |
| 20 | 528.1 | 5138.2 | 103.9 | 6.4 | 275.7 | 79.3 |
| 25 | 555.8 | 5358.5 | 109.0 | 6.1 | 258.6 | 77.1 |
| 30 | 573.0 | 5551.5 | 115.9 | 5.9 | 246.1 | 74.8 |
| 35 | 591.3 | 5682.3 | 120.2 | 5.8 | 240.8 | 73.6 |
| 40 | 596.7 | 5800.4 | 126.6 | 5.6 | 235.9 | 74.6 |
| 45 | 611.7 | 5899.4 | 131.4 | 5.4 | 230.8 | 75.1 |
| 50 | 638.9 | 6071.5 | 139.0 | 5.8 | 236.9 | 77.5 |
| 55 | 650.5 | 6255.9 | 148.0 | 5.8 | 235.8 | 78.0 |
| 60 | 666.0 | 6412.9 | 151.8 | 5.6 | 234.2 | 78.4 |

[a] $H_3Cit$: 0.4 mol $L^{-1}$; flow rate: 30 ml $min^{-1}$.

Published on 03 August 2020. Downloaded on 9/3/2025 6:59:12 AM.

continuous manufacturing is an unavoidable step before the practical application. Therefore, this research is believed to be beneficial and significant to the sustainable development of continuous leaching of LIB cathode materials in the future.

## Conclusions

Continuous hydrothermal leaching of $LiCoO_2$ with $H_3Cit$ was successfully achieved using a specially designed and customized flow system. Prior to the hydrothermal acid leaching experiment, a three-layer model was used to predict the flow state in this flow system, and a cold flow test using two kinds of flow lines was performed to determine the conditions in the preliminary experiments. From the viewpoints of suppressing the deposition and improving the operability, the pulp density of the slurry and the flow rate were set to 10 g $L^{-1}$ and 30 ml $min^{-1}$, respectively, and the position of feeding tanks was rearranged. In the first run of continuous hydrothermal leaching of $LiCoO_2$ with $H_3Cit$, the leaching efficiency of Li and Co reached 81.3% and 92.7%, respectively, at 60 min after the start of slurry feeding, and is expected to increase even after 60 min. It is promising to continuously obtain the recovered solution or leachate with a high leaching efficiency by continuing the operation, indicating that the continuous hydrothermal leaching process is feasible and promising to be applied. Except for Li and Co, other metal ions were detected in the recovered solution, which was proven to originate from the stainless steel used in the flow system. Meanwhile, the acid corrosion caused by $H_3Cit$ was revealed, which is expected to be resolved by using inner coating materials with high acid corrosion resistance or organic acids with low or no acid corrosion as the leachant.

## Conflicts of interest

There are no conflicts to declare.

## Acknowledgements

This work was supported by the Japan Science and Technology Agency (JST)-Mirai program [grant number JP18077450] and the Japan Society for the Promotion of Science (JSPS)-Grant-in-Aid for Challenging Exploratory Research [grant number No. 18K18966].

## Notes and references

1 Y. Nishi, *J. Power Sources*, 2001, **100**, 101–106.
2 B. Scrosati, J. Hassoun and Y. K. Sun, *Energy Environ. Sci.*, 2011, **4**, 3287–3295.
3 W. Gao, J. Song, H. Cao, X. Lin, X. Zhang, X. Zheng, Y. Zhang and Z. Sun, *J. Cleaner Prod.*, 2018, **178**, 833–845.
4 J. W. Fergus, *J. Power Sources*, 2010, **195**, 939–954.
5 C. Liu, J. Lin, H. Cao, Y. Zhang and Z. Sun, *J. Cleaner Prod.*, 2019, **228**, 801–813.
6 M. K. Jha, A. Kumari, A. K. Jha, V. Kumar, J. Hait and B. D. Pandey, *Waste Manage.*, 2013, **33**, 1890–1897.
7 C. K. Lee and K.-I. Rhee, *J. Power Sources*, 2002, **109**, 17–21.
8 M. Chen, X. Ma, B. Chen, R. Arsenault, P. Karlson, N. Simon and Y. Wang, *Joule*, 2019, **3**, 2622–2646.
9 F. Gu, P. A. Summers and P. Hall, *J. Cleaner Prod.*, 2019, **237**, 117657.
10 R. Golmohammadzadeh, F. Faraji and F. Rashchi, *Resour., Conserv. Recycl.*, 2018, **136**, 418–435.
11 Q. Meng, Y. Zhang and P. Dong, *J. Cleaner Prod.*, 2018, **180**, 64–70.
12 X. Chen, C. Luo, J. Zhang, J. Kong and T. Zhou, *ACS Sustainable Chem. Eng.*, 2015, **3**, 3104–3113.
13 X. Zheng, Z. Zhu, X. Lin, Y. Zhang, Y. He, H. Cao and Z. Sun, *Engineering*, 2018, **4**, 361–370.
14 D. A. Ferreira, L. M. Z. Prados, D. Majuste and M. B. Mansur, *J. Power Sources*, 2009, **187**, 238–246.
15 P. Meshram, Abhilash, B. D. Pandey, T. R. Mankhand and H. Deveci, *JOM*, 2016, **68**, 2613–2623.
16 L. Li, W. Qu, X. Zhang, J. Lu, R. Chen, F. Wu and K. Amine, *J. Power Sources*, 2015, **282**, 544–551.
17 L. Li, J. B. Dunn, X. X. Zhang, L. Gaines, R. J. Chen, F. Wu and K. Amine, *J. Power Sources*, 2013, **233**, 180–189.
18 L. Li, J. Ge, F. Wu, R. Chen, S. Chen and B. Wu, *J. Hazard. Mater.*, 2010, **176**, 288–293.
19 F. Meng, Q. Liu, R. Kim, J. Wang, G. Liu and A. Ghahreman, *Hydrometallurgy*, 2020, **191**, 105160.
20 G. P. Nayaka, J. Manjanna, K. V. Pai, R. Vadavi, S. J. Keny and V. S. Tripathi, *Hydrometallurgy*, 2015, **151**, 73–77.
21 S. Natarajan, A. B. Boricha and H. C. Bajaj, *Waste Manage.*, 2018, **77**, 455–465.
22 L. Li, E. Fan, Y. Guan, X. Zhang, Q. Xue, L. Wei, F. Wu and R. Chen, *ACS Sustainable Chem. Eng.*, 2017, **5**, 5224–5233.
23 L.-P. He, S.-Y. Sun, Y.-Y. Mu, X.-F. Song and J.-G. Yu, *ACS Sustainable Chem. Eng.*, 2017, **5**, 714–721.
24 X. Zeng, J. Li and B. Shen, *J. Hazard. Mater.*, 2015, **295**, 112–118.
25 G. P. Nayaka, K. V. Pai, G. Santhosh and J. Manjanna, *J. Environ. Chem. Eng.*, 2016, **4**, 2378–2383.
26 T. Aikawa, M. Watanabe, T. M. Aida and R. L. Smith Jr, *Kagaku Kogaku Ronbunshu*, 2017, **43**, 313–318.
27 L. Li, J. Lu, Y. Ren, X. X. Zhang, R. J. Chen, F. Wu and K. Amine, *J. Power Sources*, 2012, **218**, 21–27.
28 D. Azuma, T. Aikawa, Y. Hiraga, M. Watanabe and R. L. Smith Jr, *Kagaku Kogaku Ronbunshu*, 2019, **45**, 147–157.
29 G. S. Calabrese and S. Pissavini, *AIChE J.*, 2011, **57**, 828–834.
30 L. Rogers and K. F. Jensen, *Green Chem.*, 2019, **21**, 3481–3498.
31 P. Doron and D. Barnea, *Int. J. Multiphase Flow*, 1993, **19**, 1029–1043.
32 P. Doron, D. Granica and D. Barnea, *Int. J. Multiphase Flow*, 1987, **13**, 535–547.


This journal is © The Royal Society of Chemistry 2020